Building Principles and Structural Motifs in TiO x Ultrathin Films on a (111) Substrate

ARTICLE *in* THE JOURNAL OF PHYSICAL CHEMISTRY C · JUNE 2012

Impact Factor: 4.77 · DOI: 10.1021/jp303730j

7 AUTHORS, INCLUDING:

Emanuele Cavaliere
Catholic University of the Sacred Heart
31 PUBLICATIONS **191** CITATIONS
SEE PROFILE

Luca Gavioli
Catholic University of the Sacred Heart
76 PUBLICATIONS **764** CITATIONS
SEE PROFILE

Gaetano Granozzi
University of Padova
301 PUBLICATIONS **4,395** CITATIONS
SEE PROFILE

Alessandro Fortunelli
Italian National Research Council
210 PUBLICATIONS **3,990** CITATIONS
SEE PROFILE

THE JOURNAL OF PHYSICAL CHEMISTRY C

Article

pubs.acs.org/JPCC

Building Principles and Structural Motifs in TiO_x Ultrathin Films on a (111) Substrate

Giovanni Barcaro,[†] Emanuele Cavaliere,[‡] Luca Artiglia,[§] Luca Sementa,[†] Luca Gavioli,[‡] Gaetano Granozzi,[§] and Alessandro Fortunelli*[,†]

[†]CNR-IPCF, Molecular Modeling Laboratory, Via G. Moruzzi 1, 56124 Pisa, Italy

[‡]Interdisciplinary Laboratories for Advanced Materials Physics (i-LAMP) and Dipartimento di Matematica e Fisica, Università Cattolica del Sacro Cuore, Via dei Musei 41, 25121 Brescia, Italy

[§]Dipartimento di Scienze Chimiche and Unità INSTM, Università di Padova, 35131 Padova, Italy

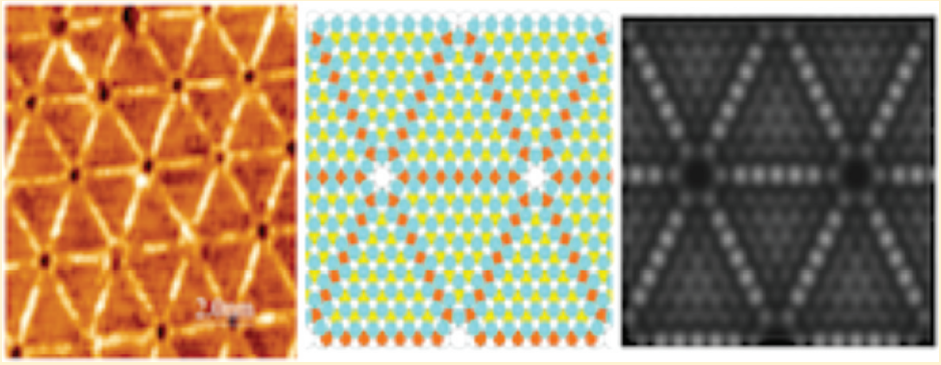

ABSTRACT: The competition between rectangular and hexagonal phases in TiO_x ultrathin (monolayer) films grown on a Pt(111) surface is discussed and rationalized on the basis of general building principles for these pseudoepitaxial oxide phases on a (111) metal substrate. A novel hexagonal reduced phase is also presented for the first time, obtained by thermal treatment at high temperature (~1000 K), and its atomistic structure is unveiled through a combination of STM experiments and theoretical simulations. A consistent picture is obtained for a class of structural families for ultrathin oxide phases on close-packed single-crystal metal surfaces.

I. INTRODUCTION

Oxide nanostructures grown on metal single-crystal supports are a subject of great interest for basic science and possible technological applications.[1,2] In this context, ultrathin (~1−2 nm thick) films play a relevant role and have been intensively studied in the past 20 years (see, for example, refs 3−6). Their conductive character and, thus, the possibility of applying surface science techniques employing charged probes have, in fact, allowed researchers to conduct in-depth investigations of structure−property relationships, so that these materials are now considered ideal systems for model studies on extended two-dimensional phases. From this work, a varied and interesting structural landscape has resulted, with a large range of possible morphologies and different configurations, ranging from flat (nonpolar) structures to strongly rumpled (thus polar) arrangements, including various combinations of these two extremes.[7,8] In general, it has not been easy to find general principles that are able to rationalize the experimental findings, even when the atomistic structures of the oxide films have been fully clarified through accompanying theoretical simulations. For example, on (111) surfaces of fcc metals, phases with both rectangular[9,10] and hexagonal[6,11−18] symmetry have been observed, but the reasons for their prevalence under different conditions are still basically unclear. However, simple rules for predicting the thermodynamically or kinetically favored structures would be very helpful to rationalize the experimental observations and orient the synthesis of these materials. For example, a topic of great current interest is the search for phases exhibiting regular arrangements of defects and thus useful as nanopatterned substrates for the preparation of ordered arrays of monodisperse nanoparticles.[19,20]

In the present work, we make a step forward in the direction of a better understanding of the interplay among structural motifs in ultrathin oxide films. We select a specific oxide/metal combination, namely, TiO_x (titanium oxide or titania) phases on the Pt(111) surface, on which a wealth of experimental and theoretical information is available,[11,21,22] and analyze prototypical examples of rectangular and hexagonal phases, additionally presenting a novel hexagonal phase here for the first time. We show that various factors determine the relative stability of these competing structural families, among which the most important ones are the stoichiometry of the oxide phase (fixed by the thermodynamic conditions) and the

Received: April 18, 2012
Published: May 29, 2012

   dx.doi.org/10.1021/jp303730j | J. Phys. Chem. C 2012, 116, 13302−13306

epitaxial relationships between the oxide and the metal components, in terms of both the lattice mismatch between the film and the substrate and the film/substrate adhesion energy. We also show that, by adjusting these factors, it is possible to obtain phases with a regular arrangement of defects positioned at different distances that can thus act as templates of ordered arrays of nanoparticles of different sizes and interparticle distances, as in the novel hexagonal phase here presented.

This article is organized as follows: In section II, the computational and experimental details are provided. Results are presented and discussed in section III, and section IV summarizes our main conclusions.

II. COMPUTATIONAL AND EXPERIMENTAL DETAILS

Spin-unpolarized density functional (DF) calculations were performed using the QuantumEspresso suite of programs,[23] employing ultrasoft pseudopotentials[24] and the PW91 exchange-correlation functional.[25] Values of 30 and 150 Ry (1 Ry = 13.606 eV) were used as the energy cutoff for the selection of the plane-wave basis set for the description of the wave function and the electronic density, respectively. A Gaussian smearing technique with a broadening of the one-particle levels of 0.03 eV was applied. A minimum distance of 8−10 Å of empty space along the direction perpendicular to the surface was inserted between replicated cells to cancel unphysical dipole interactions. As the present titania phases exhibit a polar character, all of the calculations were performed by adding a dipole correction[26] for the correct evaluation of energies and forces on a system composed of an asymmetric unit cell made of two metal slabs with the oxide layer deposited on one of them. The calculations were performed at the Γ point only, as it has been validated that this does not introduce a substantial loss of accuracy with respect to the use of a finer k_{mesh} grid for the sampling of the first Brillouin zone.[9] The DF local relaxations were performed by fully relaxing the coordinates of the oxide atoms until the forces were smaller than 0.01 eV/Å per atom, whereas the Pt atoms of the two layers used to describe the metal support were left frozen in the crystal sites of the bulk metal fcc structure with a lattice constant corresponding to the experimental value (first-neighbor distance of 2.775 Å). Simulated scanning tunneling microscopy (STM) images were obtained using the Tersoff−Hamann[27] approach at a height corresponding to about 2 Å above the average position of the oxygen layer. Values of 10^{-4}−10^{-5} au for the isosurface density contours were used.

rect-z′ and h(9 × 9) films were grown in an ultra-high-vacuum (UHV) preparation chamber ($P < 2 \times 10^{-10}$ mbar) and then analyzed in situ in an analysis chamber equipped with a UHV Omicron Multiscan Lab setup ($P < 5 \times 10^{-11}$ mbar). In more detail, in the preparation chamber, a Pt(111) substrate was cleaned by repeated cycles of sputtering with an Ar ion beam at 1 keV and annealing up to 1000 K, followed by slow (1 K/s) cooling, to yield a sharp (1 × 1) low-energy electron diffraction (LEED) pattern and no surface contamination as detected by X-ray photoelectron spectroscopy (XPS). The deposition of the z′-TiO_x phase was performed at room temperature in an oxygen background [$p(O_2) = 10^4$ Pa] using electron-beam evaporation from a Ti wire. The z′-TiO_x phase can be obtained with a Ti dose of 0.8 ML equivalent (MLE), whereas 1 MLE corresponds to 1.5×10^{15} at. cm^2, as determined with a quartz microbalance after an annealing at approximately 673 K. The h(9 × 9) reconstruction was obtained after UHV annealing of the clean rect-z′ phase at 1000 K. STM images were recorded at room temperature in an Omicron VT-STM system operating at a base pressure of 5×10^{-9} Pa. The system was equipped with a four-grid LEED optics. PtIr tips were used in all experiments, and tunneling voltages are given with respect to the sample. The tunneling parameters are reported in the corresponding captions of the reported STM images.

III. RESULTS AND DISCUSSION

We start the discussion by reviewing some general building principles of reduced titania ultrathin phases on (111) metal substrates that will be useful to rationalize the observed behavior and findings.

Building Principles. In general, when supported on an M(111) surface (M = Pd, Pt, Au, etc.),[5,11,12,17,28] reduced TiO_x phases tend to grow according to a quasihexagonal pseudomorphic polar arrangement exhibiting an M−Ti−O stacking sequence, that is, with the Ti ions at the interface with the support and the O ions forming the topmost overlayer. This is a general tendency of polar phases of ultrathin oxides on (111) metal supports, whence the interest in TiO_x phases as model systems. If the lattice parameters of the metal support and the polar oxide phase were the same, the Ti atoms could form a perfect monolayer occupying one-half of the fcc/hcp hollow sites above the Pt(111) surface, and the O ions could form a perfect monolayer occupying one-half of the hcp/fcc hollow sites of the Ti monolayer. This hypothetical TiO phase with 1:1 stoichiometry does not form for two reasons: (i) The stoichiometry of the oxide (namely, the ratio between the numbers of O and Ti atoms) favored by the given thermodynamic conditions is usually larger than 1. (ii) There is a mismatch between the lattice constants of the metal support and the oxide layer. Concerning point ii, it should be recalled that, in principle, the optimal lattice parameter of the oxide film differs from that of the bulk oxide because of both its nanoscopic (ultrathin) character and the oxide/substrate interaction.[29] Moreover, the oxide lattice parameter can also be a function of the stoichiometry of the phase. In the present case, we found that the lattice parameters of titania monolayers supported on Pt(111) are similar for both the $TiO_{1.25}$ and $TiO_{1.14}$ phases to be discussed herein and that they are, on average, slightly larger than those of the bulk phases at the corresponding stoichiometry because of the interaction with the substrate.[10] A way to solve this mismatch problem[9] is to create quasihexagonal (111) islands of finite extension separated by dislocation lines. Inside each island, the Ti ions are surrounded by three O ions (tricoordinated, Ti_3, species), whereas along the dislocation lines, the Ti ions are surrounded by four O ions (tetra-coordinated, Ti_4, species); see Figure 1b,d,f, in which z′-TiO_x/Pt(111) phases are reported. (This information is elaborated from previous works.[10,21]) The Ti atoms in two nearest-neighbor Ti_3 islands are located in stacking fault positions: If the Ti atoms (O atoms) on one side of the dislocation line are located in the fcc sites of the Pt(111) surface, then on the other side, the Ti atoms (O atoms) will be located in hcp sites, and vice versa. It can also be noted that the Ti_3 ions within the islands are located in quasihollow fcc sites, whereas the Ti_4 ions at the dislocation lines are located in bridge sites between two metal atoms of the underlying metal support. Through the formation of such dislocation lines, the number of O ions can exceed the number of Ti ions (achieving the required stoichiometry), and at the same time, the oxide

dx.doi.org/10.1021/jp303730j | J. Phys. Chem. C 2012, 116, 13302−13306

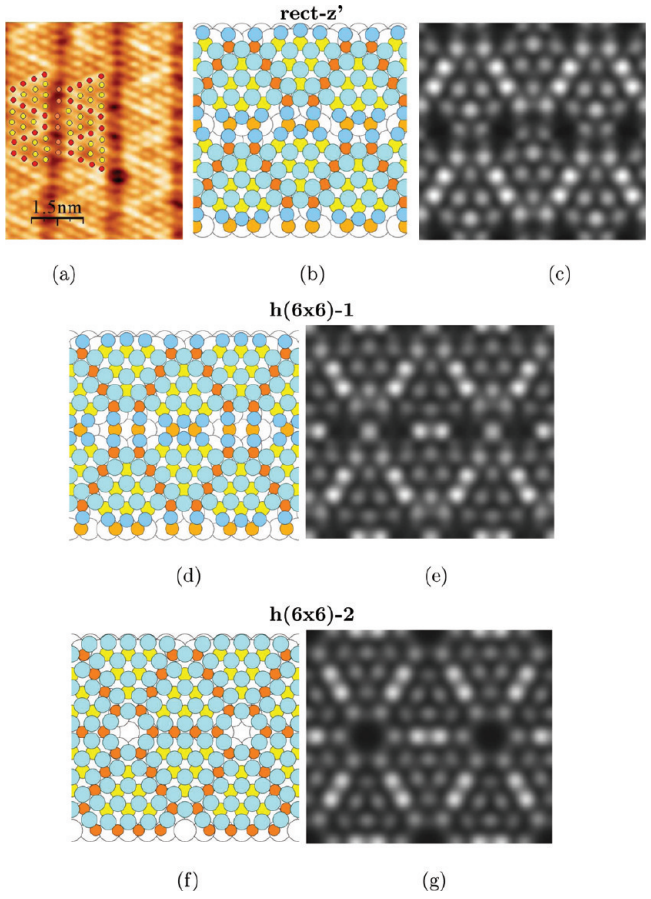

Figure 1. (a) Experimental STM image at a positive bias of +1.0 V, (b) structural DFT model and (c) simulated STM image of the rect-z′ phase at a positive bias of +1.0 V.[10] (d,f) Structural DFT models and (e,g) STM simulated images of the (d,e) h(6 × 6)-1 and (f,g) h(6 × 6)-2.[21] Ti_3 atoms are marked by yellow dots. Ti_4 atoms are marked by red dots. Ti atoms in the trough are depicted in orange. O atoms inside the stripes are depicted in light blue, whereas those in the troughs in dark blue. Pt atoms are depicted in white.

manages to release the stress generated by the lattice mismatch. The size of the Ti_3 islands is governed by the overall stoichiometry of the oxide film and also by the lattice mismatch with the metal substrate. As the (111) Ti_3 islands correspond to regions where the oxide stoichiometry is 1:1, we expect that more reduced stoichiometries will lead to the formation of larger islands. In terms of nomenclature, we label these reduced phases according to the size of the islands or, equivalently, the number of Ti_4 ions that form the boundaries of the (111) islands. For example, a (6 × 6) phase is formed by (111) Ti_3 islands containing six Ti_3 atoms and surrounded by boundary dislocation lines each containing six Ti_4 ions. It is shown in the following discussion that the island boundaries are quite often not perfectly geometric, lacking some atoms (usually the vertices; see the discussion about the hexagonal phases) or entire sides (as, for example, in the case of the rect-z′ phase), but for their nomenclature, we refer to their ideal geometries.

It should finally be noted that, in the STM images at positive bias, the Ti ions appear as bright spots, as the density of states (DOS) above the Fermi level is dominated by the unoccupied d states of the oxidized Ti ions in a range of several electronvolts.[9] Among these, the Ti_4 species appear brighter, as they are more strongly oxidized than the Ti_3 species and thus have a higher density of empty states above the Fermi level (see Figure 1).

We now discuss selected titania reduced phases on Pt(111), starting with a review of the available information on the rectangular and hexagonal z′ phases.

rect-z′ and h(6 × 6) Phases. The structure of the rect-z′ phase has been the subject of a deep experimental and theoretical investigation.[10] An experimental STM image of this phase is shown in Figure 1a, whereas its atomistic structure and a simulated STM image at positive bias are shown in parts b and c, respectively, of Figure 1. The rect-z′ phase exhibits a rectangular unit cell measuring 16.65 × 14.42 Å, and it is formed by small (111) islands made of six Ti_3 atoms separated by dislocation lines (two per triangle) formed by four Ti_4 atoms per side. [Note, however, that two Ti_4 atoms are missing, so that this is really a rect(6 × 6) phase.] The islands are organized in stripes running along the direction parallel to the long side of the unit cell and are separated by dark troughs with some extra Ti atoms filling the troughs, except for two oval-shaped cavities per unit cell.

More precisely, the atoms in the troughs can be divided into two groups that alternate with the oval cavities.[30] Each group is formed by two Ti atoms and five O atoms: On one side of the trough, the two Ti atoms are pinned to the two Ti_4 atoms that end the two dislocations surrounding the same island. On the other side of the trough, the same two Ti atoms naturally continue the arrangement of the Ti_3 atoms of the island. The two groups can be transformed into each other through a rotation of 180° plus a translation of one-half period.

The rectangular phase can be transformed into two different, but nearly iso-energetic, hexagonal phases: the h(6 × 6)-1 and h(6 × 6)-2 phases, shown in Figure 1d–g, along with their atomistic structures and STM images simulated at positive bias. The two hexagonal unit cells (side length of 16.65 Å) have the same surface area as the rect-z′ phase, but they differ in the arrangement of the Ti atoms in the trough. Note that, in the rect-z′ phase, two first-neighbor stripes can be obtained from each other by a translation operation, whereas in the hexagonal phases, two first-neighbor stripes are mirrored into each other by a plane located along the trough direction. This fact is important in understanding the structures of these phases. The h(6 × 6)-1 unit cell presents three cavities (not very different from the oval cavities of the rect-z′ phase[30]); see Figure 1d. For h(6 × 6)-2, instead the Ti atoms have rearranged their positions, closing the two oval cavities and forming a new circular (and larger) hole in correspondence with the 6-fold symmetry axis of the hexagonal unit cell. From Figure 1g, one can see that the boundaries surrounding Ti_3 islands are defective: In principle, they should be formed by six Ti_4 ions, but the three Ti atoms at the crossing of the boundaries are missing to create the hexagonal cavities. Hence, each side is formed by only four Ti_4 atoms corresponding to four bright spots in the simulated STM image. The h(6 × 6)-1 and h(6 × 6)-2 phases are nearly degenerate, lying about 0.5 eV per unit cell higher in energy than the rect-z′ phase, and, indeed, it is the latter phase that is experimentally observed for proper values of the Ti coverage and thermodynamic conditions, namely, $p(O_2) \approx 10^{-10}$ mbar and $T \approx 700$ K.[11] The stoichiometry of the rect-z′ phase is $TiO_{1.25}$, as the unit cell contains 24 Ti atoms and 30 O atoms, and coincides with that of the h(6 × 6)-1 and h(6 × 6)-2 phases.

h(9 × 9) phase. If one anneals the rect-z′ phase at temperatures higher than 700 K, a reduction of the oxide is

dx.doi.org/10.1021/jp303730j | J. Phys. Chem. C 2012, 116, 13302–13306

expected by oxygen loss upon progressive heating, as for bulk systems.[31] Indeed, this is what we actually found: An experimental STM image shown in Figure 2a, obtained after

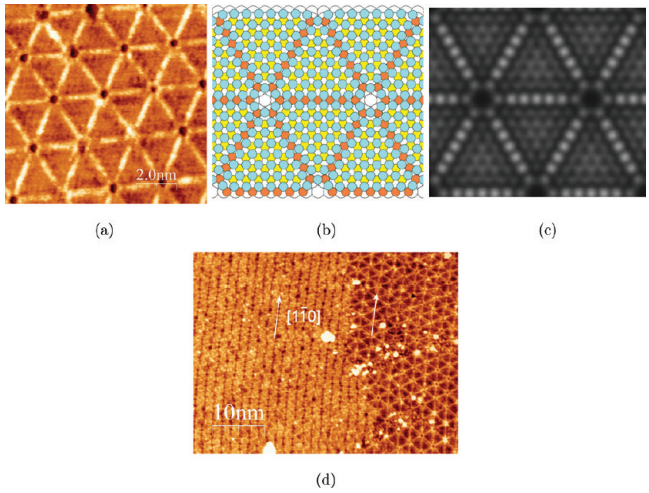

Figure 2. (a) Experimental STM image (10 nm × 10 nm, V = +0.21 V, I = 1.22 nA), (b) structural DFT model and (c) simulated STM image of the h(9 × 9) phase at a positive bias of +1.0 V. Ti_3 atoms are depicted in yellow, Ti_4 atoms in red, and O atoms in light blue. (d) Experimental STM image at a positive bias of +1.0 V in a region of coexistence between the h(9 × 9) and rect-z′ phases.

heating the z′ phase at ∼1000 K and a pressure of $p(O_2) < 10^{-10}$ mbar (UHV conditions) for 30 min, shows that a novel hexagonal phase is produced by the thermal treatment, with a lattice parameter of about 2.5 nm (the distance between the black holes at the centers of the hexagons). Such a lattice constant and the STM pattern suggest that this structure corresponds to an h(9 × 9) phase, and indeed, by setting up the geometry for such a phase and performing the calculation, we found the DF-optimized structure and STM image simulated at positive bias shown in parts b and c, respectively, of Figure 2, where the STM image is in excellent agreement with the experimental observations.

The proposed structural model is further supported by the experimental STM measurement shown in Figure 2d, where, under appropriate conditions, a coexistence between the rect-z′ and h(9 × 9) phases was observed. The figure shows that the troughs of the rect-z′phase are aligned with one of the symmetry directions (dislocation lines) of the h(9 × 9) phase, in perfect agreement with theoretical modeling. The precise interface between the two phases also excludes the possibility of incommensurate Moirè phases. The stoichiometry of this new phase is $TiO_{1.14}$, as the h(9 × 9) unit cell contains 63 Ti atoms and 72 O atoms and the (111) islands are formed by 21 Ti_3 atoms. A change in the oxide stoichiometry has thus determined a change in the overall structure of the film. It can be observed that the average lattice constants of the oxide are about the same in the two hexagonal phases, as the unit cell of the h(9 × 9) structure is larger by a factor 1.5 × 1.5 = 2.25 than the h(6 × 6) cell (1.5 = 9/6). One can estimate the Gibbs free energy of the reaction corresponding to the oxide reduction as

$$TiO_{1.25} \rightarrow TiO_{1.14} + 0.055O_2(g)$$

According to our DFT energetics, the energy of this reaction amounts to about +0.25 eV. Under the hyphothesis of ideal-gas behavior, the Gibbs free energy of molecular oxygen at T = 1000 K and a partial pressure of about 10^{-10} mbar amounts to 4.80 eV. The Gibbs free energy of the reaction is thus slightly negative, explaining the preference for the reduced $TiO_{1.14}$ stoichiometry under these thermodynamic conditions.

Summary. Let us thus summarize the results of the previous analysis. To achieve great structural stability, various requirements should be fulfilled for reduced TiO_x phases on Pt(111). First, the given experimental conditions (primarily, the temperature, but also the oxygen pressure) determine the overall stoichiometry of the film. The Ti/O ratio and, to a lesser degree, the lattice mismatch between reduced titania and platinum, in turn, determine the sizes of the pseudoepitaxial Ti_3 island and the corresponding Ti_4 dislocation lines (i.e., the length of the sides of the Ti_3 triangles). On a substrate such fcc Pt(111), pseudomorphic patterns of Ti_3 ions in quasihollow sites on the surface enhance the adhesion of the oxide to the substrate. However, the length of the sides of the Ti_3 triangular islands should match an integer number of Pt−Pt lattice parameters; otherwise, rotated Moiré phases, with an appreciably smaller oxide/substrate interaction, would be produced. All of these requirements are satisfied for triangles with sides of 6 and 9, corresponding to Ti/O ratios of 1.25 and 1.14, respectively. However, a further requirement holds for rectangular phases, for which there is an energy penalty for an odd length of the Ti_3 triangles, due to the fact that Ti_2O_5 units are favored within the troughs (see the discussion above), entailing an even number of Ti ions along the cell boundaries. At the $TiO_{1.25}$ stoichiometry, the rect-z′ phase is thus realized, which is more stable than the h(6 × 6) phase because of the perfect matching and alignment of the troughs along the (100) directions of the substrate. At the $TiO_{1.14}$ stoichiometry, instead, the odd number of Ti atoms along the cell side definitively disfavors the rectangular arrangement, and a hexagonal motif is realized in the h(9 × 9) phase.

Finally, it can be stressed that both the rect-z′ and h(6 × 6) and h(9 × 9) phases exhibit picoholes that can act as trapping centers for growing species.[30] The main difference among them is the distance between these picoholes, namely, ∼16 Å for the rect-z′ and h(6 × 6) phases and ∼25 Å for the h(9 × 9) phase. The h(9 × 9) phase can thus be used when a larger distance between the templated particles is desired.

IV. CONCLUSIONS

The structure of oxide ultrathin films grown on metal substrates is a topic of great relevance in modern surface science because of its relationships to the novel properties exhibited by these exotic phases. In this context, on (111) metal surfaces, a large number of possible configurations have been reported in the literature using microscopic techniques with atomistic resolution, and their structures have been clarified in several cases with the help of theoretical calculations. Among all of these structures, the ones having regular arrays of defects that can act as heterogeneous nucleation centers for the growth of further adsorbants (such as metal clusters) are particularly intriguing as examples of self-organized surface nanopatterning and in view of producing ordered arrays of adsorbed nanoparticles. To move with a rationale in the vast set of different morphologies, some building principles are in order. In the present work, we have proposed a rationale for the vast set of different morphologies and structural motifs observed for ultrathin oxide films on (111) substrates. We have shown through a combined theoretical and experimental analysis that general

dx.doi.org/10.1021/jp303730j | J. Phys. Chem. C 2012, 116, 13302−13306

building principles can explain the competitive interplay of rectangular and hexagonal phases exhibited by reduced titania ultrathin films on Pt(111). In this way, new phases can be designed and predicted a priori, and these predictions can be confirmed in actual experiments.[32] These hexagonal phases are particularly interesting, as they contain picoholes at the symmetry points exhibiting oxide vacancies that can act as trapping centers for growing adsorbed species. For example, the h(6 × 6)-2 and h(9 × 9) phases investigated here present "sieves" with distances of ∼16 and ∼25 Å, respectively. We believe that these findings will support and stimulate further research in this fascinating field.

AUTHOR INFORMATION

Corresponding Author

*E-mail: alessandro.fortunelli@cnr.it.

Notes

The authors declare no competing financial interest.

ACKNOWLEDGMENTS

A.F. acknowledges financial support from the EC VII FP within the ERC-AG SEPON project (ERC-2008-AdG-227457). G.G. acknowledges financial support from by the Italian Ministry of Instruction, University and Research (MIUR) through FIRB Project RBAP115AYN, "Oxides at the Nanoscale: Multifunctionality and Applications", and through the fund Programs of National Relevance (PRIN-2009). Calculations were performed at the CINECA Center (Bologna, Italy) within the ISCRA Programme.

REFERENCES

(1) Kolmakov, A.; Moskovits, M. *J. Am. Chem. Soc.* **2004**, *34*, 151.
(2) Rodriguez, J. A.; Ma, S.; Liu, P.; Hrbek, J.; Evans, J.; Perez, M. *Science* **2007**, *318*, 1757.
(3) Chen, M. S.; Goodman, D. W. *J. Phys.: Condens. Matter* **2008**, *20*, 264013.
(4) Freund, H.-J. *Surf. Sci.* **2007**, *601*, 1438.
(5) Wu, Q. H.; Fortunelli, A.; Granozzi, G. *Int. Rev. Phys. Chem.* **2009**, *28*, 517.
(6) Surnev, S.; Ramsey, M. G.; Netzer, F. P. *Prog. Surf. Sci.* **2003**, *73*, 117.
(7) Gubo, M.; Ebensperger, C.; Meyer, W.; Hammer, L.; Heinz, K. *J. Phys.: Condens. Matter* **2009**, *21*, 474211.
(8) Gragnaniello, L.; Agnoli, S.; Parteder, G.; Barolo, A.; Bondino, F.; Allegretti, F.; Surnev, S.; Granozzi, G.; Netzer, F. *Surf. Sci.* **2010**, *604*, 2002.
(9) Barcaro, G.; Fortunelli, A.; Sedona, F.; Granozzi, G. *J. Phys. Chem. C* **2007**, *111*, 6095.
(10) Sedona, F.; Granozzi, G.; Barcaro, G.; Fortunelli, A. *Phys. Rev. B* **2008**, *77*, 115417.
(11) Sedona, F.; Rizzi, G. A.; Agnoli, S.; Xamena, F. X. L. I.; Papageorgiou, A.; Ostermann, D.; Sambi, M.; Finetti, P.; Schierbaum, K.; Granozzi, G. *J. Phys. Chem. B* **2005**, *109*, 24411.
(12) Wu, C.; Marshall, M. S. J.; Castell, M. R. *J. Phys. Chem. C* **2011**, *115*, 8643.
(13) Bardi, U.; Atrei, A.; Rovida, G. *Surf. Sci.* **1992**, *268*, 87.
(14) Zhang, L.; van Ek, J.; Diebold, U. *Phys. Rev. B* **1998**, *57*, R4285.
(15) Nilius, N.; Wallis, T. M.; Ho, W. *Phys. Rev. Lett.* **2003**, *90*, 046808.
(16) Stacchiola, D.; Kaya, S.; Weissenrieder, J.; Kuhlenbeck, H.; Shaikhutdinov, S.; Freund, H.-J.; Sierka, M.; Todorova, T. K.; Sauer, J. *Angew. Chem., Int. Ed.* **2006**, *45*, 7636.
(17) Bowker, M.; Stone, P.; Morrall, P.; Smith, R.; Bennett, R.; Perkins, N.; Kvon, R.; Pang, C.; Fourre, E.; Hall, M. *J. Catal.* **2005**, *234*, 172.
(18) Bennett, R. A.; Pang, C. L.; Perkins, N.; Smith, R. D.; Morrall, P.; Kvon, R. I.; Bowker, M. *J. Phys. Chem. B* **2002**, *106*, 4688.
(19) Brune, H. *Surf. Sci. Rep.* **1998**, *31*, 121.
(20) Gavioli, L.; Cavaliere, E.; Agnoli, S.; Barcaro, G.; Fortunelli, A.; Granozzi, G. *Prog. Surf. Sci.* **2011**, *86*, 59.
(21) Barcaro, G.; Agnoli, S.; Sedona, F.; Rizzi, G. A.; Fortunelli, A.; Granozzi, G. *J. Phys. Chem. C* **2009**, *113*, 5721.
(22) Cavaliere, E.; Artiglia, L.; Barcaro, G.; Rizzi, G. A.; Bondino, F.; Fortunelli, A.; Gavioli, L.; Granozzi, G. *Phys. Chem. Chem. Phys.* **2011**, *13*, 17171.
(23) Giannozzi, P.; Baroni, S.; Bonini, N.; Calandra, M.; Car, R.; Cavazzoni, C.; Ceresoli, D.; Chiarotti, G. L.; Cococcioni, M.; Dabo, I.; Dal Corso, A.; de Gironcoli, S.; Fabris, S.; Fratesi, G.; Gebauer, R.; Gerstmann, U.; Gougoussis, C.; Kokalj, A.; Lazzeri, M.; Martin-Samos, L.; Marzari, N.; Mauri, F.; Mazzarello, R.; Paolini, S.; Pasquarello, A.; Paulatto, L.; Sbraccia, C.; Scandolo, S.; Sclauzero, G.; Seitsonen, A.P.; Smogunov, A.; Umari, P.; Wentzcovitch, R.M. *J. Phys.: Condens. Matter* **2009**, *21*, 395502.
(24) Vanderbilt, D. *Phys. Rev. B* **1990**, *41*, 7892.
(25) Perdew, J. P.; Chevary, J. A.; Vosko, S. H.; Jackson, K. A.; Pederson, M. R.; Singh, D. J.; Fiolhais, C. *Phys. Rev. B* **1992**, *46*, 6671.
(26) Bengtsson, L. *Phys. Rev. B* **1999**, *59*, 12301.
(27) Tersoff, J.; Hamann, D. R. *Phys. Rev. Lett.* **1983**, *50*, 1998.
(28) Song, Z.; Hrbek, J.; Osgood, R. *Nano Lett.* **2005**, *5*, 1327.
(29) Barcaro, G.; Thomas, I. O.; Fortunelli, A. *J. Chem. Phys.* **2010**, *132*, 124703.
(30) Artiglia, L.; Cavaliere, E.; Vascon, A.; Bondino, F.; Rizzi, G. A.; Gavioli, L.; Granozzi, G. *J. Phys. Chem. C* **2011**, *115*, 15812.
(31) Bowker, M.; Bennett, A. *J. Phys.: Condens. Matter* **2009**, *21*, 474224.
(32) Sierka, M. *Prog. Surf. Sci.* **2010**, *85*, 398.